

# Effective Diffusivity in Baroclinic Flow

ERIC M. LEIBENSPERGER<sup>\*†</sup> AND R. ALAN PLUMB

*Program in Atmospheres, Oceans, and Climate, Department of Earth, Atmospheric and Planetary Sciences*

*Massachusetts Institute of Technology, Cambridge, Massachusetts*

---

<sup>\*</sup>Now at Center for Earth and Environmental Science, State University of New York at Plattsburgh

<sup>†</sup>*Corresponding author address:* 101 Broad Street, Plattsburgh, NY 12901.

E-mail: eric.leibensperger@plattsburgh.edu

## ABSTRACT

Large-scale chaotic stirring stretches tracer contours into filaments containing fine spatial scales until small-scale diffusive processes dissipate tracer variance. Quantification of tracer transport in such circumstances is possible through the use of Nakamura’s “effective diffusivity” diagnostics, which make clear the controlling role of stirring, rather than small-scale dissipation, in large-scale transport. Existing theory of effective diffusivity is based on a layerwise approach, in which tracer variance is presumed to cascade via horizontal (or isentropic) stirring to small-scale horizontal (or isentropic) diffusion. In most geophysical flows of interest, however, baroclinic shear will tilt stirred filamentary structures into almost-horizontal sheets, in which case the thinnest dimension is vertical; accordingly, it will be vertical (or diabatic) diffusion that provides the ultimate dissipation of variance. Here we present theoretical developments to define effective diffusivity in such flows. In the frequently relevant case of isentropic stirring, we show that the theory is in most respects unchanged from the case of isentropic diffusion: effective isentropic diffusivity is controlled by the isentropic stirring and, it is argued, is largely independent of the nature of the ultimate dissipation. Diabatic diffusion is not amplified by the stirring, although it can be modestly enhanced through eddy modulation of static stability. These characteristics are illustrated in numerical simulations of a stratospheric flow; in regions of strong stirring the theoretical predictions are well supported, but agreement is less good where stirring is weaker.

# 1. Introduction

Transport of tracers in large-scale atmospheric and oceanic flows is often described as a two-dimensional process, in which, through chaotic stirring, tracer variance cascades down to small scales at which diffusion — whether via molecular or small-scale turbulent processes — takes effect. A particularly clear and useful quantitative description of transport in a given two-dimensional flow was given by Nakamura (1996, 1998) (hereinafter N96, N98) (and also by Winters and D’Asaro (1996)) who showed that, in a two-dimensional cascade to ultimate two-dimensional diffusivity  $\kappa$ , net transport is diffusive with an “effective diffusivity”  $K_{eff} = \alpha\kappa$ , where  $\alpha$  is proportional to the square of the ratio of the “equivalent length” of tracer contours to their reference (unstretched) length. Under chaotic advection, tracer contours are stretched by the strain in the flow and  $\alpha$  becomes large. The arrest of the variance cascade occurs at the “Batchelor scale”  $b \sim \sqrt{\kappa/S}$ , when thinning of tracer filaments by the large-scale strain  $S$  is balanced by small-scale diffusion. For sufficiently small  $b$ , one expects the length of tracer contours to be proportional to  $b^{-1}$  (so as to preserve area) and hence the equivalent length to vary as  $\kappa^{-1/2}$ . Then,  $K_{eff}$  becomes independent of  $\kappa$  and transport is controlled by large-scale stirring rather than by small-scale diffusion (Shuckburgh and Haynes 2003; Marshall et al. 2006). Application of this theory to modeled and observed atmospheric flows has been discussed by Nakamura and Ma (1997), Haynes and Shuckburgh (2000a), Haynes and Shuckburgh (2000b), Allen and Nakamura (2001), and Kostykin and Schmitz (2006), and to oceanic flows by Marshall et al. (2006), Cerovecki et al. (2009), and Abernathy et al. (2010).

In almost all circumstances, however, the underlying framework of these calculations is not a realistic representation of the termination of the cascade in large-scale atmospheric and oceanic flows. While such flows are indeed almost two-dimensional (in the sense of being quasi-horizontal or quasi-isentropic) they are usually also baroclinic. As the isentropic strain effects a cascade of tracer variance to small horizontal scales, the vertical shear tilts such features in the tracer field (see Fig. 2) such that the expected ratio of vertical to horizontal

scales, in balanced flow, scales as the Prandtl ratio  $f/N$ , the ratio of the Coriolis parameter to the buoyancy frequency [e.g., Haynes and Anglade (1997)]. In the atmosphere, and in the upper ocean,  $f/N$  is typically of order  $10^{-2}$ ; vertical scales are therefore much smaller than horizontal scales. Thus, what appear to be filaments on an isentropic cross-section are more likely to be vertically thin, quasi-horizontal layers. Fig. 1 shows an example of such a feature simulated by the atmospheric model described in Section 3a. The feature has a much narrower vertical than horizontal extent, displaying a tilt approximately equal to the local value of Prandtl's ratio (dashed line in Fig. 1).

The cascade produced by such large-scale quasi-isentropic stirring is typically arrested by small-scale diffusion that is more isotropic than the large-scale flow. Whenever the ratio of diabatic to isentropic diffusivities is greater than the square of the aspect ratio of filamentary structures, *i.e.*,  $(f/N)^2$ , vertical (diabatic) diffusion will dominate the dissipation of variance by acting on the small vertical scales (as indicated in Fig. 2). In this paper, we investigate the implications of this fact for our theories of large-scale transport. It is argued that for a given large-scale flow the horizontal (isentropic) effective diffusivity will be independent of whether  $\kappa$  acts horizontally or vertically.

A related, and equally important, question is whether the effects of large-scale stirring and tilting enhance transport across, as well as within, isentropic surfaces. Fig. 2 might suggest that diabatic transport is enhanced by the generation of small vertical scales. Given the potential importance of even a modest augmentation of the effects of small-scale diabatic transport in stably stratified environments like the stratosphere or the ocean, where diabatic transport is otherwise weak, the question is an important one.

Theoretical developments, including the derivation of an expression for the net isentropic transport (based on the formalism of Nakamura, but with some minor modifications) for the case in which the cascade of tracer variance is arrested by isotropic diffusion, are presented in Section 2. The predictions of this theory are illustrated by results from explicit numerical simulations of tracer transport in a modeled stratosphere in Section 3. We conclude in

76 Section 4 by discussing the general applicability of our results and their implications for the  
77 numerical representation of tracer transport.

## 78 2. Theory

79 We begin by considering a tracer  $q$ , governed by the advection-diffusion equation

$$\frac{\partial q}{\partial t} + \mathbf{u}_h \cdot \nabla q + \dot{\theta} \frac{\partial q}{\partial \theta} = \dot{q} \quad (1)$$

80 where  $\dot{q}$  represents the diffusion that ultimately dissipates tracer variance at small scales.  
81 N96 and N98 considered the case where this diffusion occurs isentropically,

$$\dot{q} = \nabla_h (\kappa_i \nabla_h q) \quad (2)$$

82 Here  $\nabla_h$  denotes the components of the gradient operator within the  $\theta$  surface and  $\kappa_i$  is the  
83 isentropic diffusivity. Our focus here is on cases where the ultimate dissipation of variance  
84 is dominated by diabatic diffusion, represented by

$$\dot{q} = \frac{1}{\sigma} \frac{\partial}{\partial \theta} \left( \kappa_d \sigma |\nabla \theta|^2 \frac{\partial q}{\partial \theta} \right) \quad (3)$$

85 where  $\kappa_d$  is the diabatic diffusivity expressed in height coordinates and  $\sigma = -g^{-1} \partial p / \partial \theta$  is  
86 the  $\theta$ -coordinate density, which itself satisfies the continuity equation

$$\frac{\partial \sigma}{\partial t} + \nabla_h \cdot (\sigma \mathbf{u}_h) + \frac{\partial}{\partial \theta} (\sigma \dot{\theta}) = 0 \quad (4)$$

87 Our analysis mostly follows the modified Lagrangian mean (MLM) approach of N96  
88 and N98, though with some minor notational changes and a somewhat different coordinate  
89 system, which makes the form of the MLM tracer budget a little more familiar. The MLM  
90 is defined along contours of constant  $q = Q$  and on a surface of constant  $\theta = \Theta$ ; N98  
91 then relabels the  $Q$  coordinate as an equivalent area coordinate  $A_e$  (to be defined below),  
92 expressing the final budget in  $(A_e, \Theta)$  coordinates. We make a further trivial step, replacing

the area coordinate with a linear variable  $Y$ , and relabeling the  $\Theta$  coordinate with the mean height  $Z$  of the  $\theta = \Theta$  surface.

Following N98, we consider density-weighted integrals over the area enclosed on a surface of constant  $\theta = \Theta$  by a contour  $q(x, y, \theta) = Q$ . For definiteness, we shall assume that the contour surrounds a maximum of  $q$ , though the end result is independent of this assumption. Defining the mass integral of any quantity  $X$  as

$$\mathcal{M}\{X\} = \iint_{q>Q} \sigma X \, dA, \quad (5)$$

the integrated mass per unit  $\Theta$  is

$$M(Q, \Theta, t) = \mathcal{M}\{1\} = \iint_{q>Q} \sigma \, dA. \quad (6)$$

Further, the “modified Lagrangian mean” — the density-weighted mean around the contour — is defined, following N96, N98, as

$$\langle X \rangle = \frac{\partial}{\partial Q} (\mathcal{M}\{X\}) \left( \frac{\partial M}{\partial Q} \right)^{-1} = \oint \sigma X \frac{dl}{|\nabla_h q|} \left[ \oint \sigma \frac{dl}{|\nabla_h q|} \right]^{-1}. \quad (7)$$

Then, again following N98, we apply the operator (5) to (4) to obtain

$$\frac{\partial M}{\partial t} + \frac{\partial}{\partial Q} [\mathcal{M}\{\dot{q}\}] + \frac{\partial}{\partial \Theta} [\mathcal{M}\{\dot{\theta}\}] = 0. \quad (8)$$

Now, we change independent variables from  $(Q, \Theta)$  to  $(Y, Z)$ . Here  $Y$  is a latitude-like coordinate, constant along a contour of constant  $(Q, \Theta)$ , defined as follows. First we follow N98 in defining an “equivalent area”  $A_e$  within a  $(Q, \Theta)$  contour such that  $M(Q, \Theta) = S(\Theta)A_e$ , where  $S(\Theta)$  is a representative isentropic density (for our purposes, we define it to be the hemispheric average of  $\sigma$  on each  $\Theta$  surface). Then we associate equivalent area with a linear coordinate  $Y$  such that  $dA_e = L(Y) \, dY$ , where  $dY = a \, d\phi_e$ ,  $\phi_e$  is the “equivalent latitude” (Butchart and Remsberg 1986), the latitude circle containing an area equal to  $A_e$ ,

$$\phi_e = \pm \sin^{-1} \left[ 1 - \frac{A_e}{2\pi a^2} \right], \quad (9)$$

110 and

$$L(Y) = \mp 2\pi a \cos \phi_e \quad (10)$$

111 is the circumference of the latitude circle. (The choice of sign depends on the hemisphere of  
 112 interest. For our purposes, we define area to be that south of the respective  $Q$  contour, and  
 113 so we choose the negative sign in (9) and correspondingly the positive sign in (10).) We  
 114 additionally define the height coordinate  $Z(\Theta)$  to be the mean (log-pressure) height of the  
 115  $\theta = \Theta$  surface.

116 It is a straightforward matter (details are given in the Appendix) to show that (8) leads  
 117 to the following advection-diffusion equation in  $(Y, Z)$  coordinates:

$$\frac{\partial Q}{\partial t} + V \frac{\partial Q}{\partial Y} + W \frac{\partial Q}{\partial Z} = \bar{\rho}^{-1} \bar{\nabla} \cdot (\bar{\rho} \mathbf{K} \bar{\nabla} Q) \quad (11)$$

118 where  $\bar{\nabla} \equiv (\partial/\partial Y, \partial/\partial Z)$ , the nondivergent advecting diabatic mean velocity is

$$\mathbf{V} = (V, W) = \frac{1}{\bar{\rho}} \left( -\frac{\partial}{\partial Z}, \frac{\partial}{\partial Y} \right) \mathcal{M} \{ \dot{\theta} \} \quad (12)$$

119 similar to N98,  $\bar{\rho}$  is the mass density in  $(Y, Z)$  coordinates (defined in Appendix A), and the  
 120 effective diffusivity tensor is

$$\mathbf{K} = \begin{pmatrix} K_{YY} & K_{YZ} \\ K_{ZY} & K_{ZZ} \end{pmatrix}. \quad (13)$$

121 For the case of ultimate isentropic diffusion (2),  $K_{YZ} = K_{ZY} = K_{ZZ} = 0$  and

$$K_{YY} = \langle \kappa_i |\nabla_h q|^2 \rangle \left( \frac{\partial Q}{\partial Y} \right)^{-2} \quad (14)$$

122 as described by N96 and N98. With diabatic diffusion (3), however, it is shown in Appendix

123 B that the effective diffusivity components are<sup>1</sup>

$$\begin{aligned}
K_{YY} &= \langle \kappa_d |\nabla\theta|^2 q_\theta'^2 \rangle \left( \frac{\partial Q}{\partial Y} \right)^{-2} = \langle \kappa_d q_z'^2 \rangle \left( \frac{\partial Q}{\partial Y} \right)^{-2}, \\
K_{YZ} &= K_{ZY} = \langle \kappa_d |\nabla\theta|^2 q_\theta' \rangle \left( \frac{\partial Q}{\partial Y} \frac{d\Theta}{dZ} \right)^{-1}, \\
K_{ZZ} &= \langle \kappa_d |\nabla\theta|^2 \rangle \left( \frac{d\Theta}{dZ} \right)^{-2},
\end{aligned} \tag{15}$$

124 where

$$q_\theta' \equiv \frac{\partial q}{\partial \theta} - \frac{\partial Q}{\partial \Theta} \tag{16}$$

125 and  $q_z' = |\nabla\theta| q_\theta'$ . Note that  $q_\theta'$  is not strictly an eddy term, as there is in general no guarantee  
126 that  $\langle q_\theta' \rangle = 0$ ; however, this quantity does in fact vanish if  $\sigma$  does not vary on isentropes,  
127 as shown in Appendix C.

128 The usefulness, and general applicability, of expressions like (14) and (15) for diffusivity  
129 rely on their independence of the details of each tracer. At first sight, the fact that (14)  
130 and  $K_{YY}$  and  $K_{YZ}$  in (15) involve tracer gradients and the small scale diffusivities might  
131 suggest otherwise. However, note that in each case the diffusivities depend on ratios of the  
132 “eddy” tracer gradients to the large-scale isentropic gradients. The former are generated by  
133 kinematic folding and tilting of the latter, suggesting that for sufficiently small diffusivity the  
134 effective diffusivities are characteristics of the large-scale flow, independent of tracer details.  
135 For Nakamura’s isentropic diffusivity (14) these issues have been discussed by N96 and, in  
136 some detail, by Shuckburgh and Haynes (2003) and Marshall et al. (2006). For sufficiently  
137 large Peclet number,  $Pe = \Lambda / (\kappa_i L_0)$ , where  $\Lambda$  is the rate of stretching by the large-scale  
138 flow and  $L_0$  a typical length scale of the flow, the cascade of tracer variance is halted at  
139 the Bachelor scale  $b \sim \sqrt{\kappa_i / \Lambda} \ll L_0$ ; in this limit the effective diffusivity  $K_{YY}$  becomes  
140 independent of the small scale diffusivity, and in fact scales as  $\Lambda L_0^2$ . Marshall et al. (2006)

---

<sup>1</sup>The definition of the various components is in fact non-unique: one can manipulate the definitions of the components of  $\mathbf{K}$  and of the advecting velocity  $\mathbf{V}$  in such a way as to leave the net transport unchanged. (One example of this ambiguity is noted in Section 3c, below.) The definition set we present here seems to be the simplest and most logical choice.



found this limit to be reached when  $Pe \gtrsim 20$ .

It is to be anticipated that similar arguments apply to the case with diabatic small-scale diffusion. In fact if we anticipate, following Haynes and Anglade (1997), the vertical and horizontal scales in a mature cascade to be in Prandtl's ratio such that  $(q'_z)^2 \sim N^2 \langle |\nabla_h q'|^2 \rangle / f^2$ , the isentropic diffusivity becomes

$$K_{YY} \simeq \langle \kappa_d q'^2_z \rangle \left( \frac{\partial Q}{\partial Y} \right)^{-2} \sim \left\langle \kappa_d \frac{N^2}{f^2} |\nabla_h q'|^2 \right\rangle \left( \frac{\partial Q}{\partial Y} \right)^{-2}.$$

Then the expression for effective isentropic diffusivity  $K_{YY}$  in the presence of ultimate vertical diffusion is formally the same as that for ultimate isentropic diffusion with an isentropic diffusivity  $\kappa_i = \kappa_d N^2 / f^2$ . The same arguments about insensitivity of  $K_{YY}$  to  $\kappa_i$  then apply as in the isentropic case, leading to the expectation that  $K_{YY}$  also becomes, in the weak diffusion limit, a measure of large-scale stretching rates. Hence, we might anticipate — and we shall illustrate in model results analyzed in Section 3 — that  $K_{YY}$  becomes largely independent of whether the ultimate dissipation of tracer variance is diabatic or isentropic.

The off-diagonal components of the diffusivity tensor indicate, if non-zero, that the principal axis of effective diffusion does not coincide with the isentropes. One can show that these components are in fact zero if there are no variations of either  $|\nabla\theta|$  or  $\sigma$  within isentropic surfaces: if variations in  $|\nabla\theta|$  along a tracer contour can be neglected then  $\langle |\nabla\theta|^2 q'_\theta \rangle = \langle |\nabla\theta|^2 \rangle \langle q'_\theta \rangle$  and, as already noted,  $\langle q'_\theta \rangle = 0$  under such circumstances. As will be shown in the next section, while these off-diagonal terms are not zero in our numerical simulations they are small enough to be of little practical consequence.

Note that the expression for vertical effective diffusivity  $K_{ZZ}$  in (15) is unrelated to the isentropic stirring and baroclinic tilting of tracer contours of the kind illustrated in Fig. 2. Enhancement of diabatic diffusion occurs only through the factor  $\langle |\nabla\theta|^2 \rangle / (d\Theta/dZ)^2$ , which is independent of the tracer structures, but rather expresses the impact of modulations of isentropic thickness by the eddies. Unlike the collapse of vertical scales of the tracer variance, there are strong dynamical constraints preventing the sustained collapse of isentropic thickness; nevertheless, the possibility of some enhancement of diabatic mixing in

the presence of eddies is indicated by (15) and will be discussed further in what follows.

### 3. Numerical Simulation of $K_{YY}, K_{YZ}, K_{ZZ}$

#### *a. Atmospheric Model*

In this section, we illustrate the theoretical results of Section 2 with simulations of atmospheric tracer transport in a simplified general circulation model. Our focus is the stratosphere, building upon prior application of the N98 framework to the middle atmosphere by Haynes and Shuckburgh (2000a), Allen and Nakamura (2001), and Kostrykin and Schmitz (2006). The model is similar to that of Polvani and Kushner (2002), consisting of a dry pseudospectral dynamical core forced by the thermodynamic and momentum parameterizations of Held and Suarez (1994). The model integrates the primitive equations within a hybrid  $\sigma - p$  vertical coordinate extending from the surface to 0.006 hPa. Simulations are conducted at the combinations of horizontal and vertical resolution listed in Table 1. Vertical resolution in the stratosphere varies from 0.8 km (100 levels) to 2.0 km (40 levels). Rayleigh friction is applied below 700 hPa to represent surface drag and above 0.5 hPa to crudely parameterize gravity wave drag within the mesosphere. Temperatures are linearly relaxed to zonal equilibrium profiles; equilibrium temperature profiles used here are similar to those of Held and Suarez (1994), but contain asymmetry about the equator to generate solstice conditions. A polar vortex is formed within the winter hemisphere by imposing a lapse rate in equilibrium temperature  $\gamma$  of  $4 \text{ K km}^{-1}$  through the polar stratosphere (Polvani and Kushner 2002). A 1000 day spin-up is conducted from a static, isothermal initial condition for each resolution.

The model transports tracers horizontally using a semi-Lagrangian advection scheme and vertically with a finite volume parabolic scheme. Mass conservation is not assured by these schemes, but we enforce it by applying a global “mass fixer.” This correction scales the tracer field after each advective timestep in order to retain a constant global tracer mass.

Test simulations conducted without the mass fixer reveal that its use does not significantly affect our calculation of effective diffusivity. The model’s tracer simulation has recently been used to diagnose stratosphere-troposphere exchange (Orbe and Polvani 2012) and the Brewer-Dobson circulation (Gerber 2012).

Two tracers, each containing no source or sink, are simulated in each model integration; small scale diffusion is applied purely isentropically to one tracer, and purely diabatically to the other. Both tracers thus experience the same large-scale stirring, but differ in the mechanism dissipating small-scale tracer variance. Additional diffusion arises from the numerical advection routines. We quantify numerical diffusion by calculating the tendency of globally averaged tracer variance (Allen and Nakamura 2001; Abernathy et al. 2010):

$$\frac{1}{2} \frac{\partial \overline{q^2}}{\partial t} = -\kappa_i^{num} \overline{|\nabla q|^2} - \kappa_v^{num} \overline{\left( \frac{\partial q}{\partial z} \right)^2}. \quad (17)$$

Here, the overbar  $\overline{(\ )}$  represents the global mass-weighted mean. We separately regress the tendency of globally averaged tracer variance against  $\overline{|\nabla q|^2}$  and  $\overline{(\partial q / \partial z)^2}$  since horizontal and vertical numerical diffusion cannot be disentangled. As a result, the estimates presented in Table 1 assume the destruction of tracer variance occurs solely through horizontal or vertical numerical diffusion and are upper limits. As might be expected, the amount of numerical diffusion is greatest for the coarsest simulations and decreases as resolution improves.

An explicit diffusivity of  $\kappa_i = 5.0 \times 10^4 \text{ m}^2 \text{ s}^{-1}$  is applied to the “isentropic” tracer and  $\kappa_d = 1.25 \text{ m}^2 \text{ s}^{-1}$  to the “diabatic tracer.” These values are larger than our estimates for numerical diffusion, though only marginally so for the diabatic tracer except in the simulations containing 100-layers. Tracer concentrations are initialized with  $q = |\phi|$  (ppb) for  $\phi < 0$ , where  $\phi$  is latitude. Elsewhere, tracer concentrations are initialized with a value of 0.01 ppb. There is no initial vertical structure in the tracer fields. Each tracer simulation is conducted for at least 100 days. The first 30 days of the tracer simulation are discarded to ensure flow diagnostics independent of the initial tracer field (Haynes and Shuckburgh 2000a).

The stratospheric circulation generated in this model, other factors being fixed, depends

on the magnitude of planetary-scale topography specified at the surface. For example, wavenumber-2 topography of amplitude 3 km generates large amplitude quasi-stationary Rossby waves sufficient to produce intermittent major warming events of realistic frequency and intensity (Gerber and Polvani 2009). Major warming events, however, are undesirable in our study since such events cause our calculated effective diffusivity to become an average over two stirring regimes: quiescent periods when stirring is mostly confined to the mid-latitude surf zone, and warming events during which stirring extends across high latitudes. Accordingly, we choose to focus our calculations on a less disturbed regime by imposing a flat lower boundary in the model. Planetary-scale Rossby waves produced by synoptic wave interactions (Scinocca and Haynes 1998) still appear in the stratosphere, but are weak enough that, at least with this model configuration, only weak, minor, warming events are produced. This is not particularly realistic as an analog of the northern winter circulation, but is qualitatively similar to the behavior of the southern stratosphere in midwinter. As we shall see, the relatively weak stirring in the middle and upper the stratosphere has some consequences for the interpretation of effective diffusivity in the results.

#### *b. Calculation of Effective Diffusivity*

Effective diffusivity ( $K_{YY}$ ,  $K_{YZ}$ ,  $K_{ZZ}$ ) is calculated using (14) and (15), and daily tracer fields. Tracer concentrations are linearly interpolated onto isentropic surfaces extending from 400K to 1500K with 15K resolution, defining the  $\Theta$  coordinate. The  $\Theta$  coordinate is also expressed as the hemispheric mean log-pressure height  $Z$  of each surface. For each isentropic surface, 250 evenly spaced  $Q$  contour levels are created between the minimum and maximum tracer concentrations. Each  $Q$  contour is mapped onto the horizontal coordinate  $Y$  through the contour equivalent area as outlined in Section 2. We find that our calculations are not particularly sensitive to the number of tracer contours or isentropic levels used.

The calculation of effective diffusivity is the product of two components: the MLM of the local tracer or  $\theta$  gradient, and the inverse square of the large-scale gradient of tracer ( $\partial Q / \partial Y$ )

or potential temperature  $(\partial\Theta/\partial Z)$ . The latter component of the effective diffusivity is a straightforward calculation using finite differences of the mapping of  $Q \rightarrow Y$  and  $\Theta \rightarrow Z$ .

The MLM of a generalized property  $\xi$  is calculated as follows. First, a mass-weighted ( $\sigma A$ , where  $A$  is the gridbox area) summation of  $\xi$  is conducted within each contour  $Q$ . A summation of the contour mass is also performed. The MLM is calculated as the ratio of the difference of the weighted summation of  $\xi$  across  $Q$  contours to the change in mass within the contours. That is, for gridded  $\xi$ :

$$\langle \xi \rangle (Q, \Theta) = \frac{\sum_{q>Q+\delta Q} \xi(i, j, \Theta) \sigma(i, j, \Theta) A(i, j) - \sum_{q>Q-\delta Q} \xi(i, j, \Theta) \sigma(i, j, \Theta) A(i, j)}{\sum_{q>Q+\delta Q} \sigma(i, j, \Theta) A(i, j) - \sum_{q>Q-\delta Q} \sigma(i, j, \Theta) A(i, j)}, \quad (18)$$

where  $i$  and  $j$  are the horizontal gridbox indices within the appropriate  $Q$  contour. (18) is a discretized version of (7). In order to apply (18), the horizontal and vertical gradients of  $q$  are calculated for each grid point and daily tracer field. (18) is additionally used to calculate the MLM of the zonal wind.

Using  $|\nabla\theta| = \partial\theta/\partial z$ , the key expressions in the first and second of the definitions (15) for  $K_{YY}$  and  $K_{YZ}$  can be written, using (16), as

$$\left\langle \left( \frac{\partial\theta}{\partial z} \right)^2 (q'_\theta)^2 \right\rangle (Q, \Theta) = \left\langle \left( \frac{\partial q}{\partial z} - \frac{\partial\theta}{\partial z} \frac{\partial Q}{\partial\Theta} \right)^2 \right\rangle$$

and

$$\left\langle \left( \frac{\partial\theta}{\partial z} \right)^2 q'_\theta \right\rangle (Q, \Theta) = \left\langle \frac{\partial\theta}{\partial z} \left( \frac{\partial q}{\partial z} - \frac{\partial\theta}{\partial z} \frac{\partial Q}{\partial\Theta} \right) \right\rangle,$$

with  $z$  denoting the local log-pressure height.

### c. Numerical Modeling Results

The left panel of Fig. 3 shows  $K_{YY,i}$ , the isentropic diffusivity calculated using (14) and the tracer modeled with isentropic diffusion, along with the MLM of the zonal wind from the simulation with the finest horizontal (T85,  $\sim 155$  km) and vertical (100 levels,  $\sim 0.8$  km) spatial resolutions. The distribution of  $K_{YY,i}$  is similar to prior estimates for austral winter

(Haynes and Shuckburgh 2000a; Allen and Nakamura 2001), but the absolute magnitude is lower in our idealized atmosphere due to the smaller amount of wave forcing from the imposed flat topography. Small values of  $K_{YY,i}$  are found in the tropics and vortex edge, the so-called “transport barriers.” Tracer contours generally have simpler geometry in these regions with correspondingly small values of effective diffusivity. Values in these regions approach the imposed small-scale diffusivity  $\kappa_i$  ( $0.5 \times 10^5 \text{ m}^2 \text{ s}^{-1}$ ). Above the lower stratosphere, the largest values of  $K_{YY,i}$  are located equatorward of the polar vortex, where mixing is strong and tracer contours are filamented within the mid-latitude “surf zone” (see Fig. 1). In fact, the largest values of  $K_{YY,i}$  are neatly confined between the vortex and the zero zonal wind line. In this region,  $K_{YY,i}$  is up to 25 times larger than  $\kappa_i$ , indicating significant contour stretching and large equivalent lengths. Higher values of  $K_{YY,i}$  are evident in a broad latitudinal region of the lower stratosphere where stronger stirring is associated with the upper extensions of synoptic-scale tropospheric eddies.

The right panel of Fig. 3 shows  $K_{YY,d}$ , the isentropic effective diffusivity calculated using (15) and the tracer with imposed diabatic diffusion. The large-scale structure of  $K_{YY,d}$  is similar to that of  $K_{YY,i}$ , *i.e.*, values are largest in the surf zone and lower stratosphere. Within the surf zone, the spatial pattern of  $K_{YY,d}$  corresponds well with the features of  $K_{YY,i}$ , including local maxima at 475 and 800K, a broad structure between 600 and 1100K, and a minimum value at 1300K. Despite the similarities in spatial structure, however,  $K_{YY,d}$  and  $K_{YY,i}$  differ in magnitude. Fig. 4 shows their ratio,  $K_{YY,d}/K_{YY,i}$ . In line with the theoretical arguments, the ratio is close to unity in the lower stratosphere, below 550K where stirring is strongest. Elsewhere,  $K_{YY,d}$  is generally at least a factor of 2 smaller than  $K_{YY,i}$  within the surf zone and much smaller in the transport barriers. This suggests that the conditions in the regions of weaker stirring have not reached those assumed in the theoretical discussion.

In the strongly stirred lower stratosphere,  $f/N$  scaling is produced as filamentary structures are rapidly stretched and tilted. It is here that  $K_{YY,d}$  is most similar to  $K_{YY,i}$ . In contrast, the largest discrepancies between  $K_{YY,i}$  and  $K_{YY,d}$  occur in regions experiencing

291 weakest stirring, *i.e.*, the transport barriers. In these locations  $Q$  contours have simple  
 292 geometry and  $|\nabla_h q|^2 \sim (\partial Q/\partial Y)^2$ , so that  $K_{YY,i} \sim \kappa_i$ . However, since there are no fine-  
 293 scale filaments to be tilted, the vertical scale collapse is weak so that  $K_{YY,d}$  is much smaller  
 294 than  $K_{YY,i}$ . In this situation, diabatic diffusion does not participate in the dissipation of  
 295 isentropically driven cascade of tracer variance. As a result, weak diabatic diffusion does  
 296 not have much impact on tracer transport in regions experiencing little wave activity.

297 Two additional factors complicate the comparison of  $K_{YY,i}$  and  $K_{YY,d}$ : the intermittency  
 298 of wave activity and the proximity of filaments to the vortex edge. Wave activity is not  
 299 continuous and thus effective diffusivity is not constant through time. As such, the values  
 300 presented in Fig. 3 represent average conditions and do not necessarily retain  $f/N$  scaling.  
 301 Also, filaments are commonly formed by stripping tracer away from the polar vortex edge. In  
 302 this situation, a portion of the length of tracer contours lies along the vortex edge, a location  
 303 with large horizontal tracer gradients, but not necessarily large vertical gradients. The  
 304 calculation of effective diffusivity along such a contour is thus partially biased by processes  
 305 not governed by  $f/N$  scaling. These complications are overcome in the lower stratosphere,  
 306 where the effects of a strong vortex are lacking and wave activity is stronger and much more  
 307 frequent.

308 Note the relatively large values of  $K_{YY,d}$  within the polar vortex, which are especially  
 309 evident in the ratio  $K_{YY,d}/K_{YY,i}$  shown in Fig. 3. These are indicative not of the stretch-  
 310 ing/tilting processes of the surf zone, but rather of the impact of small values of  $q'_\theta$  in the  
 311 presence of the small values of  $(\partial Q/\partial Y)$  in the calculation of  $K_{YY,d}$ . Such values are in-  
 312 evitable near the pole where the mean gradient vanishes. As such, these large values of  $K_{YY,d}$   
 313 exemplify the ambiguities in the representation of  $\mathbf{K}$  noted earlier. Even in the absence of  
 314 zonal asymmetries, a vertical diffusive flux

$$\mathbf{F} = -\kappa_z \frac{\partial q}{\partial z} \hat{\mathbf{z}},$$

315 where  $\hat{\mathbf{z}}$  is the upward unit vector, can be written, identically, as the sum of a component

316 along the  $q$  contours (which is therefore advective in nature) and a horizontal component:

$$\mathbf{F} = \kappa_z \left( \frac{\partial q / \partial z}{\partial q / \partial y} \right) \hat{\mathbf{x}} \times \nabla q - \kappa_z \left( \frac{\partial q / \partial z}{\partial q / \partial y} \right)^2 \frac{\partial q}{\partial y} \hat{\mathbf{y}}, \quad (19)$$

317 where  $\hat{\mathbf{x}}$  and  $\hat{\mathbf{y}}$  are respectively unit vectors in the  $x$ - and  $y$ - directions. Thus, a vertical  
 318 diffusion can be represented by the sum of an advective flux, plus horizontal diffusion. That  
 319 this is not generally a sensible thing to do is evidenced by the fact that the transfer coefficients  
 320 in (19) are dependent on the geometry of the tracer isopleths. Provided the isopleth slopes  
 321 are dictated by the large-scale flow — as they will be in a region of strong stirring — the  
 322 effective diffusivity is meaningful. This is not the case in the weakly stirred vortex interior,  
 323 and so the relatively large polar values of  $K_{YY,d}$  are misleading. However, given the small  
 324 absolute values of  $K_{YY}$  within the vortex, the point is moot.

325 Estimates of  $K_{YY}$  are sensitive to the resolution of tracer advection: as resolution im-  
 326 proves, finer-scale features are resolved and the contour equivalent length increases (Allen  
 327 and Nakamura 2001). If the discrepancies between  $K_{YY,i}$  and  $K_{YY,d}$  are due to inade-  
 328 quate resolution of the tracer cascade, one would expect the values to show convergence as  
 329 resolution is improved. Note that changes in resolution in these calculations apply to the  
 330 dynamical fields as well as to the tracers, *i.e.*, the dynamical simulations change somewhat  
 331 as resolution is changed (although changes in the flow statistics are modest). Thus, unlike  
 332 some previous studies, the sensitivity to resolution discussed here is not simply a matter of  
 333 changing the resolution of tracer transport in a given flow.

334 The left panels of Fig. 5 show  $K_{YY,i}$  at 850K and 450K for the resolutions listed in Table  
 335 1. In order to ensure meaningful comparisons,  $K_{YY,i}$  is averaged over periods (typically 30  
 336 days) containing an active surf zone ( $K_{YY,i}$  is large). While  $K_{YY,i}$  increases with horizontal  
 337 resolution, it is not as sensitive to improved vertical resolution (dashed lines in Fig. 5). This  
 338 sensitivity is largest in the surf zone where stirring is modestly vigorous and the represen-  
 339 tation of filamentary structures benefits from enhanced resolution (Haynes and Shuckburgh  
 340 2000a; Allen and Nakamura 2001). The right panels of Fig. 5 show the effect of resolution  
 341 on the diagnosed value of  $K_{YY,d}$ . Similar to  $K_{YY,i}$ , higher resolution increases the estimate



of  $K_{YY,d}$ ; not surprisingly, in this case the greater sensitivity is to vertical resolution with a large increase between 60 levels (1.5 km) and 80 levels (1.0 km) at 850K and between 80 and 100 levels at 450K, where the length scales are smaller. Agreement between  $K_{YY,i}$  and  $K_{YY,d}$  improves with increased resolution; at the highest resolutions used here, agreement is good at 450K but at 850K the discrepancies, though smaller than at lower resolution, remain substantial.

Fig. 6 shows  $K_{YZ}$  and  $K_{ZZ}$  calculated from the same simulation presented in Fig. 3. The left panel of Fig. 6 shows  $K_{YZ}$ , the off-diagonal component of the effective diffusion tensor (15). Unlike  $K_{YY}$ ,  $K_{YZ}$  has mixed sign throughout the stratosphere. The largest values of up to  $80 \text{ m}^2 \text{ s}^{-1}$  occur in the lower stratosphere; in the middle and upper stratosphere, typical values are around  $10 \text{ m}^2 \text{ s}^{-1}$ . As mentioned in Section 2, theory suggests  $K_{YZ}$  to be negligible if variations in  $\sigma$  are small within an isentropic surface and, indeed, these values are small. The role of the off-diagonal components is to rotate the principal axes of diffusion through an angle of  $K_{YZ}/K_{YY} \sim 10^{-5}$ , which corresponds to a slope of the principal diffusion axis relative to isentropes of about 100 m between equator and pole, which can undoubtedly be regarded as negligible (isentropic surfaces themselves slope by factors of 10 – 100 more than this.)

The right panel of Fig. 6 shows that  $K_{ZZ} \approx \kappa_d$  throughout most of the stratosphere, indicating that the enhancement of tracer diffusion due to modulations of isentropic thickness by the eddies is minimal in those places.  $K_{ZZ}$  is amplified by a factor of up to 5 within the polar vortex, but this amplification appears not to be primarily the result of eddy effects. Rather,  $K_{ZZ}$  is artificially enhanced as a consequence of using the hemispheric mean height  $Z$ . Isentropic thickness is smaller within the polar vortex than elsewhere, making  $\partial\theta/\partial z > \partial\theta/\partial Z$ . As a result,  $K_{ZZ}$  is amplified there due to our choice of coordinate system rather than a physical process. Where the eddies are stronger, diabatic diffusivity is not substantially enhanced; thus it appears that the presence of eddies does not significantly enhance diabatic mixing in these simulations.

The final component of transport is mean advection. The advecting velocity that appears in (11) and in N98 has MLM mass streamfunction

$$\mathcal{M}(Y, Z, t)\{\dot{\theta}\} = \iint \sigma \dot{\theta} dA \quad (20)$$

where the integral is over the area poleward of the appropriate equivalent latitude contour (of constant  $Q$ ). This is not the same as the conventional zonal-mean diabatic circulation, which has mass streamfunction also given by (20) but for which the integral is over the area poleward of a circle of constant latitude. The two streamfunctions are compared in Fig. 7. In magnitude and in general shape, the two are similar, though the MLM streamfunction is flatter in the surf zone (with little upwelling or downwelling between 20 and 50° equivalent latitude) and the MLM high-latitude descent closely follows the vortex edge, including the equatorward kink in the edge near 500 K (compare the MLM wind maximum in Fig. 3).

## 4. Discussion

We have expanded the effective diffusivity diagnostic of N96 and N98 by deriving the equations in the presence of diabatic diffusion. Our derivation produces a solution (11) similar to that of N98, but with the isentropic effective diffusivity (denoted  $K_{YY}$ ) replaced by an effective diffusivity tensor  $\mathbf{K}$ .  $\mathbf{K}$  includes not only the isentropic component of effective diffusivity, but additionally consists of vertical ( $K_{ZZ}$ ) and off-diagonal components ( $K_{YZ}$ ). Our numerical simulations confirm the theoretical expectation that  $K_{YZ}$  is small enough to be negligible, while  $K_{ZZ}$  differs little from the imposed diabatic diffusivity  $\kappa_d$ ; thus, diabatic diffusion is not significantly modified by large-scale stirring. The first key statement to be concluded from this analysis is that large-scale tracer transport, summarized in  $K_{YY}$ , is predominantly isentropic and a property of large scale stirring; it is largely independent of the direction of dissipation (isentropic or diabatic). In practice, resolution limitations, and our choice of flow regime, rendered our simulations capable of confirming insensitivity to the nature of small-scale dissipation only in regions (the lower stratosphere) where eddy stirring

is sufficiently strong.

The second key statement is that, despite considerations raised in the Introduction in the context of Fig. 2, the tilting of stretching filaments by the baroclinic shear does not lead to augmented diabatic transport. The only impact of the eddy motions on diabatic diffusivity occurs through modulation of isentropic thickness. This could be important in situations where eddies strongly modulate static stability, and where modest augmentation of diabatic diffusion could be important. Note, however, that the discussions here are based on a constant small-scale diabatic diffusivity; if this is a turbulent process, small-scale mixing could be suppressed where static stability is locally increased, in which case  $K_{ZZ}$  may be even less sensitive to eddy effects

Our numerical simulations have focused on tracer transport in the atmosphere, but the theoretical developments are general and can be applied to all baroclinic geophysical flows large enough to be balanced. For example, oceanic tracers are also stretched into tilted filaments containing a mean aspect ratio of  $f/N$ . Smith and Ferrari (2009) simulated the cascade of thermohaline variance in a quasigeostrophic model and, similar to this work, showed that isotropic diffusive processes acting upon small vertical scales is sufficient to halt the laterally driven cascade of tracer variance, thus supporting the conclusions drawn here and highlighting the importance of compact vertical scales in the atmosphere and ocean.

Many dynamical models have been constructed with the assumption of horizontal dissipation of tracer variance. While our results indicate that these models have not correctly simulated the physical processes terminating the variance cascade, the equivalence of properly scaled isentropic or diabatic diffusion suggests that the error is not particularly egregious. However, vertical processes cannot be neglected. Even though quasi-horizontal strain drives the cascade of tracer variance, without vertical resolution sufficient to adequately resolve the ultimate dissipation of variance, the cascade will terminate too rapidly and overly dampen tracer spectra.

*Acknowledgments.*

The authors wish to thank Daniela Domeisen (University of Hamburg) and Gang Chen (Cornell University) for helpful discussions and assistance with model simulations. This work was supported by the National Science Foundation through grant ATM-0852384.

## APPENDIX A

### The advective terms

Given  $M(Q, \Theta, t) = S(\Theta)A_e(Q, \Theta, t)$  and  $(\partial A_e / \partial Y)_\Theta = L(Y)$ , we have  $dM|_\Theta = S dA_e = SL dY$ , and

$$\left. \frac{\partial}{\partial Q} \right|_\Theta = \left( \frac{\partial Q}{\partial Y} \right)_Z^{-1} \left. \frac{\partial}{\partial Y} \right|_Z \quad (\text{A1})$$

$$\left. \frac{\partial}{\partial \Theta} \right|_Q = \frac{dZ}{d\Theta} \left( \left. \frac{\partial}{\partial Z} \right|_Y - \frac{\partial Q / \partial Z}{\partial Q / \partial Y} \left. \frac{\partial}{\partial Y} \right|_Z \right) \quad (\text{A2})$$

Now,

$$\left( \frac{\partial M}{\partial t} \right)_{Q, \Theta} = - \left( \frac{\partial M}{\partial Q} \right)_\Theta \left( \frac{\partial Q}{\partial t} \right)_{Y, \Theta} = -SL \left( \frac{\partial Y}{\partial Q} \right)_\Theta \left( \frac{\partial Q}{\partial t} \right)_{Y, \Theta}.$$

Hence (8) becomes

$$\begin{aligned} \left( \frac{\partial Q}{\partial t} \right)_Y &= \left( \frac{\partial M}{\partial Q} \right)_\Theta^{-1} \left( \frac{\partial}{\partial Q} \mathcal{M} \{ \dot{q} \} \right)_\Theta + \frac{1}{SL} \left( \frac{\partial Q}{\partial Y} \right)_\Theta \left( \frac{\partial}{\partial \Theta} \mathcal{M} \{ \dot{\theta} \} \right)_Q \\ &= \langle \dot{q} \rangle + \frac{1}{SL} \left( \frac{\partial Q}{\partial Y} \right)_\Theta \left( \frac{\partial}{\partial \Theta} \mathcal{M} \{ \dot{\theta} \} \right)_Q \end{aligned} \quad (\text{A3})$$

from (7). But, using (A2)

$$\frac{d\Theta}{dZ} \left( \frac{\partial}{\partial \Theta} \mathcal{M} \{ \dot{\theta} \} \right)_Q = \left( \frac{\partial}{\partial Z} \mathcal{M} \{ \dot{\theta} \} \right)_Y - \left( \frac{\partial Q / \partial Z}{\partial Q / \partial Y} \right) \left( \frac{\partial}{\partial Y} \mathcal{M} \{ \dot{\theta} \} \right)_Z.$$

Then (A3) becomes

$$\left( \frac{\partial Q}{\partial t} \right)_Y = \langle \dot{q} \rangle - V \left( \frac{\partial Q}{\partial Y} \right)_Z - W \left( \frac{\partial Q}{\partial Z} \right)_Y \quad (\text{A4})$$

where the nondivergent advecting velocity is

$$\mathbf{V} = (V, W) = \left( -\bar{\rho}^{-1} \frac{\partial}{\partial Z} \mathcal{M} \{ \dot{\theta} \}, \bar{\rho}^{-1} \frac{\partial}{\partial Y} \mathcal{M} \{ \dot{\theta} \} \right)$$

where

$$\bar{\rho} = SL \frac{d\Theta}{dZ} = \frac{\partial M}{\partial Y} \frac{d\Theta}{dZ} \quad (\text{A5})$$

is the mass density in  $(Y, Z)$  space.

## APPENDIX B

### The diabatic diffusion term

From (7),

$$\begin{aligned} \left( \frac{\partial M}{\partial Q} \right)_\Theta \langle \dot{q} \rangle &= \frac{\partial}{\partial Q} (\mathcal{M} \{ \dot{q} \})_\Theta \\ &= \frac{\partial}{\partial Q} \left( \iint \frac{\partial}{\partial \theta} \left( \kappa_d \sigma |\nabla \theta|^2 \frac{\partial q}{\partial \theta} \right) dA \right)_\Theta \end{aligned}$$

Now, using the identity

$$\begin{aligned} \frac{\partial}{\partial \Theta} \left[ \iint X dA \right]_Q &= \iint \frac{\partial X}{\partial \theta} dA - \frac{\partial}{\partial Q} \left[ \iint X \frac{\partial q}{\partial \theta} dA \right]_\Theta \\ &= \iint \frac{\partial X}{\partial \theta} dA - \oint X \frac{\partial q}{\partial \theta} \frac{dl}{|\nabla_h q|}, \end{aligned} \quad (\text{B1})$$

we have

$$\begin{aligned} \left( \frac{\partial M}{\partial Q} \right)_\Theta \langle \dot{q} \rangle &= \frac{\partial}{\partial Q} \left[ \frac{\partial}{\partial \Theta} \left( \iint \kappa_d \sigma |\nabla \theta|^2 \frac{\partial q}{\partial \theta} dA \right)_\Theta + \oint \kappa_d \sigma |\nabla \theta|^2 \left( \frac{\partial q}{\partial \theta} \right)^2 \frac{dl}{|\nabla_{\theta q}|} \right]_\Theta \\ &= \frac{\partial}{\partial \Theta} \oint \kappa_d \sigma |\nabla \theta|^2 \frac{\partial q}{\partial \theta} \frac{dl}{|\nabla_{\theta q}|} + \frac{\partial}{\partial Q} \oint \kappa_d \sigma |\nabla \theta|^2 \left( \frac{\partial q}{\partial \theta} \right)^2 \frac{dl}{|\nabla_{\theta q}|} \\ &= \frac{\partial}{\partial \Theta} \left( \frac{\partial M}{\partial Q} \left\langle \kappa_d |\nabla \theta|^2 \frac{\partial q}{\partial \theta} \right\rangle \right) + \frac{\partial}{\partial Q} \left( \frac{\partial M}{\partial Q} \left\langle \kappa_d |\nabla \theta|^2 \left( \frac{\partial q}{\partial \theta} \right)^2 \right\rangle \right). \end{aligned}$$

Map this into  $(Y, Z)$  space using (A1) and (A2), which after some manipulation gives

$$\begin{aligned} \langle \dot{q} \rangle &= \frac{1}{\bar{\rho}} \frac{\partial}{\partial Y} \left( \bar{\rho} \left( \frac{\partial Q}{\partial Y} \right)_\Theta^{-1} \left\langle \kappa_d |\nabla \theta|^2 \frac{\partial q}{\partial \theta} \left( \frac{\partial q}{\partial \theta} - \frac{\partial Q}{\partial \Theta} \right) \right\rangle \right)_Z \\ &\quad + \frac{1}{\bar{\rho}} \frac{\partial}{\partial Z} \left( \bar{\rho} \frac{dZ}{d\Theta} \left\langle \kappa_d |\nabla \theta|^2 \frac{\partial q}{\partial \theta} \right\rangle \right)_Y. \end{aligned} \quad (\text{B2})$$

Now write  $\partial q / \partial \theta = \partial Q / \partial \Theta + q'_\theta$ . Then

$$\begin{aligned} \langle \dot{q} \rangle &= \bar{\rho}^{-1} \frac{\partial}{\partial Y} \left( \bar{\rho} \left[ \frac{\langle \kappa_d |\nabla \theta|^2 q_\theta'^2 \rangle}{(\partial Q / \partial Y)^2} \frac{\partial Q}{\partial Y} + \frac{\langle \kappa_d |\nabla \theta|^2 q'_\theta \rangle}{(\partial Q / \partial Y) (d\Theta / dZ)} \frac{\partial Q}{\partial Z} \right] \right) \\ &\quad + \bar{\rho}^{-1} \frac{\partial}{\partial Z} \left( \bar{\rho} \left[ \frac{\langle \kappa_d |\nabla \theta|^2 q'_\theta \rangle}{(\partial Q / \partial Y) (d\Theta / dZ)} \frac{\partial Q}{\partial Y} + \frac{\langle \kappa_d |\nabla \theta|^2 \rangle}{(d\Theta / dZ)^2} \frac{\partial Q}{\partial Z} \right] \right). \end{aligned} \quad (\text{B3})$$

Together, (4) and (B3) lead directly to (11).

**Proof that  $\langle q'_\theta \rangle = 0$  when  $\sigma = \sigma(\theta)$**

If  $\sigma$  is constant within the isentropic surface, we can write  $\sigma = S(\Theta)$  and so, using (6),

$$SA_e = M = \iint \sigma \, dA = S \iint dA$$

But, from (B1),

$$\begin{aligned} \frac{\partial}{\partial \Theta} \left( \iint dA \right)_Q &= - \oint \frac{\partial q}{\partial \theta} \frac{dl}{|\nabla_h q|} \\ &= - \frac{1}{S} \oint \sigma \frac{\partial q}{\partial \theta} \frac{dl}{|\nabla_h q|} \\ &= - \frac{1}{S} \left\langle \frac{\partial q}{\partial \theta} \right\rangle \left( \frac{\partial M}{\partial Q} \right)_\Theta, \end{aligned}$$

and hence

$$\left\langle \frac{\partial q}{\partial \theta} \right\rangle = - \frac{(\partial A_e / \partial \Theta)_Q}{(\partial A_e / \partial Q)_\Theta} = \left( \frac{\partial Q}{\partial \Theta} \right)_{A_e}.$$

Hence

$$\langle q'_\theta \rangle = \left\langle \frac{\partial q}{\partial \theta} \right\rangle - \left( \frac{\partial Q}{\partial \Theta} \right)_{A_e} = 0.$$

## REFERENCES

- 454 Abernathy, R., J. Marshall, M. Mazloff, and E. Shuckburgh, 2010: Enhancement of mesoscale  
 455 eddy stirring at steering levels in the Southern Ocean. *J. Phys. Oceanogr.*, **40** (1), 170–184,  
 456 doi:10.1175/2009JPO4201.1.
- 457 Allen, D. R. and N. Nakamura, 2001: A seasonal climatology of effective diffusivity in the  
 458 stratosphere. *J. Geophys. Res.*, **106** (D8), 7917–7935.
- 459 Butchart, N. and E. E. Remsberg, 1986: The area of the stratospheric polar vortex as a  
 460 diagnostic for tracer transport on an isentropic surface. *J. Atmos. Sci.*, **43** (13), 1319–  
 461 1339.
- 462 Cerovecki, I., R. A. Plumb, and W. Heres, 2009: Eddy transport and mixing in a wind- and  
 463 buoyancy-driven jet on the sphere. *J. Phys. Oceanogr.*, **39** (5), 1133–1149, doi:10.1175/  
 464 2008JPO3596.1.
- 465 Gerber, E. P., 2012: Stratospheric versus tropospheric control of the strength and struc-  
 466 ture of the Brewer-Dobson circulation. *J. Atmos. Sci.*, **69**, 2857–2877, doi:10.1175/  
 467 JAS-D-11-0341.1.
- 468 Gerber, E. P. and L. M. Polvani, 2009: Stratosphere-troposphere coupling in a relatively  
 469 simple agcm: The importance of stratospheric variability. *J. Climate*, **22** (8), 1920–1933,  
 470 doi:10.1175/2008JCLI2548.1.
- 471 Haynes, P. and J. Anglade, 1997: The vertical-scale cascade in atmospheric tracers due to  
 472 large-scale differential advection. *J. Atmos. Sci.*, **54** (9), 1121–1136.
- 473 Haynes, P. and E. Shuckburgh, 2000a: Effective diffusivity as a diagnostic of atmospheric  
 474 transport - 1. Stratosphere. *J. Geophys. Res.*, **105** (D18), 22,777–22,794.



475 Haynes, P. and E. Shuckburgh, 2000b: Effective diffusivity as a diagnostic of atmospheric  
 476 transport - 2. Troposphere and lower stratosphere. *J. Geophys. Res.*, **105** (D18), 22,794–  
 477 22,810.

478 Held, I. M. and M. J. Suarez, 1994: A proposal for the intercomparison of the dynamical cores  
 479 of atmospheric general circulation models. *Bull. Amer. Met. Soc.*, **75** (10), 1825–1830.

480 Kostykin, S. V. and G. Schmitz, 2006: Effective diffusivity in the middle atmosphere  
 481 based on general circulation model winds. *J. Geophys. Res.*, **111**, D02 304, doi:10.1029/  
 482 2004JD005472.

483 Marshall, J., E. Shuckburgh, H. Jones, and C. Hill, 2006: Estimates and implications of  
 484 surface eddy diffusivity in the southern ocean derived from tracer transport. *J. Phys.*  
 485 *Oceanogr.*, **36**, 1806–1821.

486 Nakamura, N., 1996: Two-dimensional mixing, edge formation, and permeability diagnosed  
 487 in an area coordinate. *J. Atmos. Sci.*, **53** (11), 1524–1537.

488 Nakamura, N., 1998: Leaky containment vessels of air: A lagrangian-mean approach to  
 489 the stratospheric tracer transport. *Dynamics of Atmospheric Flows: Atmospheric Trans-*  
 490 *port and Diffusion Processes*, Computational Mechanics Publications, Advances in Fluid  
 491 Mechanics, Vol. 18.

492 Nakamura, N. and J. Ma, 1997: Modified lagrangian-mean diagnostics of the stratospheric  
 493 polar vortices - 2. Nitrous oxide and seasonal barrier migration in the cryogenic limb array  
 494 etalon spectrometer and SKYHI general circulation model. *J. Geophys. Res.*, **102** (D22),  
 495 25,721–25,735.

496 Orbe, C. and L. M. Polvani, 2012: Flux distributions as robust diagnostics of stratosphere-  
 497 troposphere exchange. *J. Geophys. Res.*, **117** (D01302), doi:10.1029/2011JD016455.

- 498 Polvani, L. M. and P. J. Kushner, 2002: Tropospheric response to stratospheric perturbations  
499 in a relatively simple general circulation model. *Geophys. Res. Lett.*, **29** (7), doi:10.1029/  
500 2001GL014284.
- 501 Scinocca, J. F. and P. H. Haynes, 1998: Dynamical forcing of stratospheric planetary waves  
502 by tropospheric baroclinic eddies. *J. Atmos. Sci.*, **55** (14), 2361–2392.
- 503 Shuckburgh, E. F. and P. H. Haynes, 2003: Diagnosing transport and mixing using a tracer-  
504 based coordinate system. *Phys. Fluids*, **15**, 3342–3357.
- 505 Smith, K. S. and R. Ferrari, 2009: The production and dissipation of compensated thermo-  
506 haline variance by mesoscale stirring. *J. Phys. Oceanogr.*, **39** (10), 2477–2501.
- 507 Winters, K. B. and E. A. D’Asaro, 1996: Diascalar flux and the rate of fluid mixing. *J. Fluid*  
508 *Mech.*, **317**, 179–193.

## 509 **List of Tables**

510	1	Simulations conducted in this study and estimates of vertical and horizontal	
511		numerical diffusion	27

TABLE 1. Simulations conducted in this study and estimates of vertical and horizontal numerical diffusion

Resolution		$\kappa_h^{num}$	$\kappa_v^{num}$
Horizontal	Vertical <sup>a</sup>	[m <sup>2</sup> s <sup>-1</sup> ]	[m <sup>2</sup> s <sup>-1</sup> ]
T42 ( $\sim 2.8^\circ$ )	80 (1.0 km)	$4.6 \times 10^3$	0.8
T63 ( $\sim 1.9^\circ$ )	40 (2.0 km)	$2.4 \times 10^3$	1.0
T63 ( $\sim 1.9^\circ$ )	60 (1.5 km)	$2.2 \times 10^3$	0.9
T63 ( $\sim 1.9^\circ$ )	80 (1.0 km)	$1.8 \times 10^3$	0.8
T63 ( $\sim 1.9^\circ$ )	100 (0.8 km)	$1.4 \times 10^3$	0.2
T85 ( $\sim 1.4^\circ$ )	80 (1.0 km)	$1.2 \times 10^3$	0.7
T85 ( $\sim 1.4^\circ$ )	100 (0.8 km)	$1.0 \times 10^3$	0.2

<sup>a</sup>Resolution in model layers and vertical spacing in the stratosphere

## List of Figures

- 1 Tracer distribution on 700K surface (left) and cross section along 180°E (right) from a simulation conducted with T85 horizontal resolution and 100 vertical levels. The dashed line represents the theoretical slope of the tilted filament, the local value of the Prandtl's ratio  $f/N$ . The tracer simulation is discussed in Section 3. 30
- 2 Illustration of the tilting of narrow filaments to generate small vertical scales. The broad arrows indicate baroclinic shear; the smaller arrows depict diabatic tracer diffusion out of the filament. 31
- 3 Effective diffusivity  $K_{YY}$  ( $\times 10^5 \text{ m}^2 \text{ s}^{-1}$ ) calculated from a simulation dissipating tracer variance with explicit isentropic ( $K_{YY,i}$ , left) or diabatic ( $K_{YY,d}$ , right) diffusion. Black contours represent the MLM of the zonal wind ( $\text{m s}^{-1}$ ); contour levels are spaced  $10 \text{ m s}^{-1}$  apart and negative values are dashed. Note the difference in colorscale between  $K_{YY,i}$  and  $K_{YY,d}$ . The simulation was performed with a horizontal resolution of T85 and 100 vertical levels. 32
- 4 Ratio of  $K_{YY,d}$  to  $K_{YY,i}$  from the simulation presented in Fig. 3. Blues (reds) indicate that  $K_{YY,d}$  is lower (higher) than  $K_{YY,i}$ . 33
- 5 Effective diffusivity ( $\times 10^5 \text{ m}^2 \text{ s}^{-1}$ )  $K_{YY,i}$  (left) and  $K_{YY,d}$  on the 850K (top) and 450K (bottom) isentropic surface as calculated from simulations with spatial resolutions: T42, 40 levels (black); T63, 60 levels (red line); T63, 100 levels (red dashed line); T85, 80 levels (blue line); T85, 100 levels (blue dashed line). Note the difference in scale between  $K_{YY,i}$  and  $K_{YY,d}$ . 34
- 6 Effective diffusivity components  $K_{YZ}$  ( $\text{m}^2 \text{ s}^{-1}$ ) and  $K_{ZZ}$  ( $\text{m}^2 \text{ s}^{-1}$ ) calculated from a simulations dissipating tracer variance with explicit diabatic diffusion  $\kappa$ . Black contours represent the MLM of the zonal wind ( $\text{m s}^{-1}$ ); contour levels are spaced  $10 \text{ m s}^{-1}$  apart and negative values are dashed. Note the nonlinear colorscale of  $K_{YZ}$ . 35

539        7    Mass streamfunctions calculated relative to tracer contours (*i.e.*, equivalent  
540           latitude; left) and latitude circles (right). 36

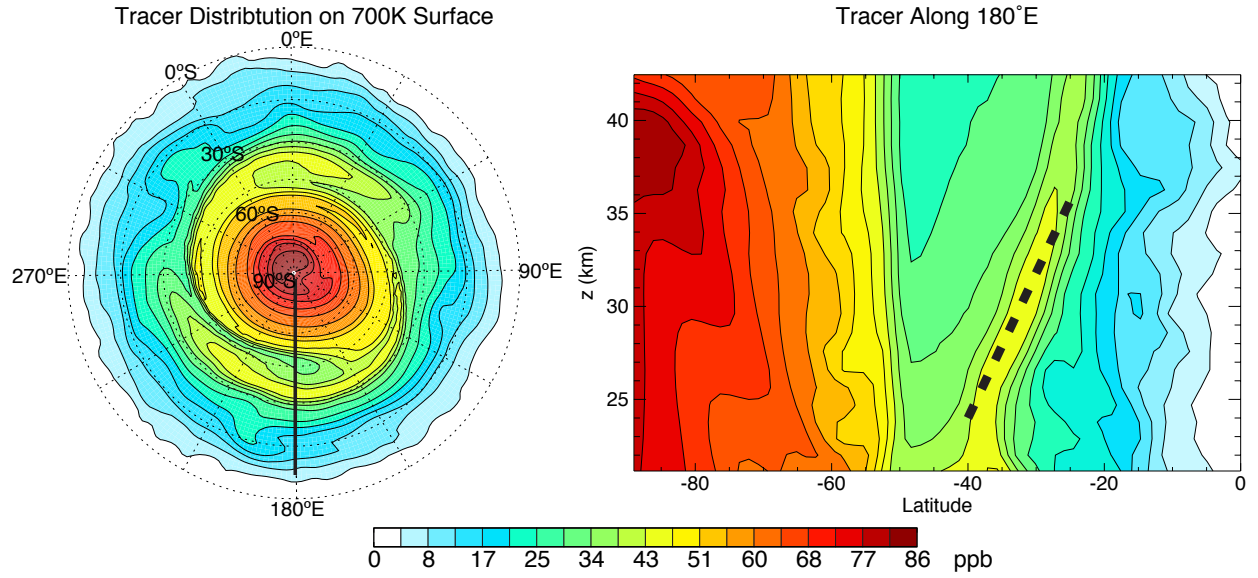


FIG. 1. Tracer distribution on 700K surface (left) and cross section along  $180^\circ\text{E}$  (right) from a simulation conducted with T85 horizontal resolution and 100 vertical levels. The dashed line represents the theoretical slope of the tilted filament, the local value of the Prandtl's ratio  $f/N$ . The tracer simulation is discussed in Section 3.

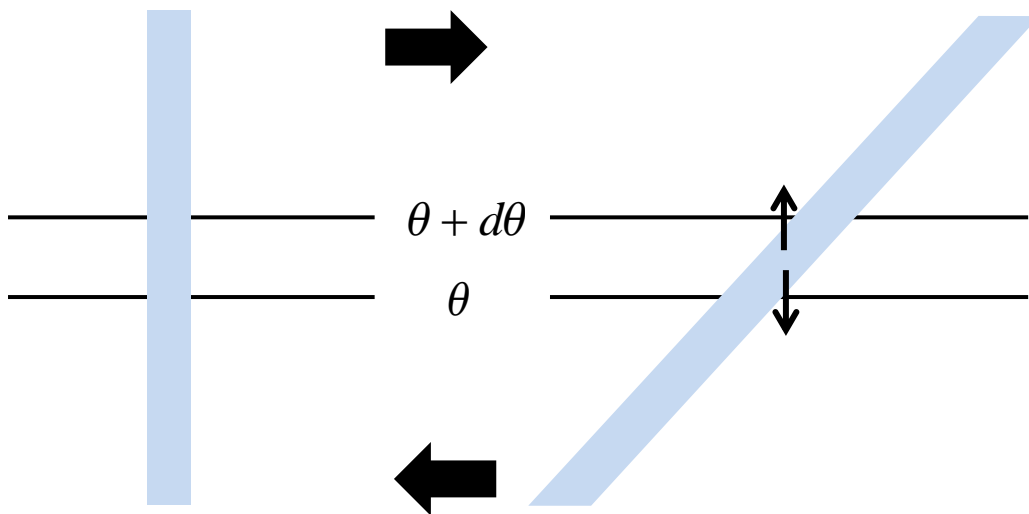


FIG. 2. Illustration of the tilting of narrow filaments to generate small vertical scales. The broad arrows indicate baroclinic shear; the smaller arrows depict diabatic tracer diffusion out of the filament.



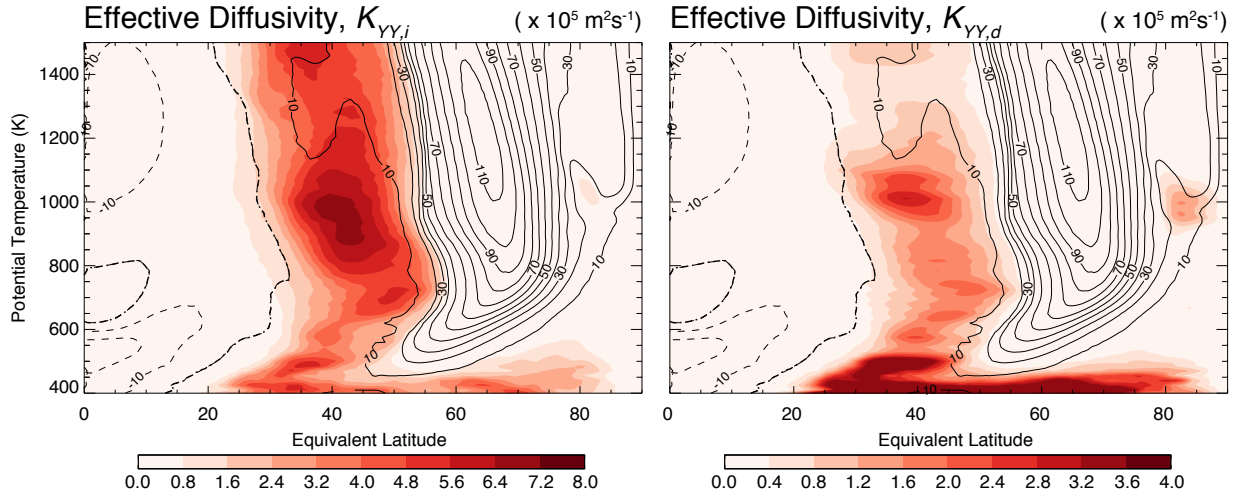


FIG. 3. Effective diffusivity  $K_{YY}$  ( $\times 10^5 \text{ m}^2 \text{ s}^{-1}$ ) calculated from a simulation dissipating tracer variance with explicit isentropic ( $K_{YY,i}$ , left) or diabatic ( $K_{YY,d}$ , right) diffusion. Black contours represent the MLM of the zonal wind ( $\text{m s}^{-1}$ ); contour levels are spaced 10  $\text{m s}^{-1}$  apart and negative values are dashed. Note the difference in colorscale between  $K_{YY,i}$  and  $K_{YY,d}$ . The simulation was performed with a horizontal resolution of T85 and 100 vertical levels.

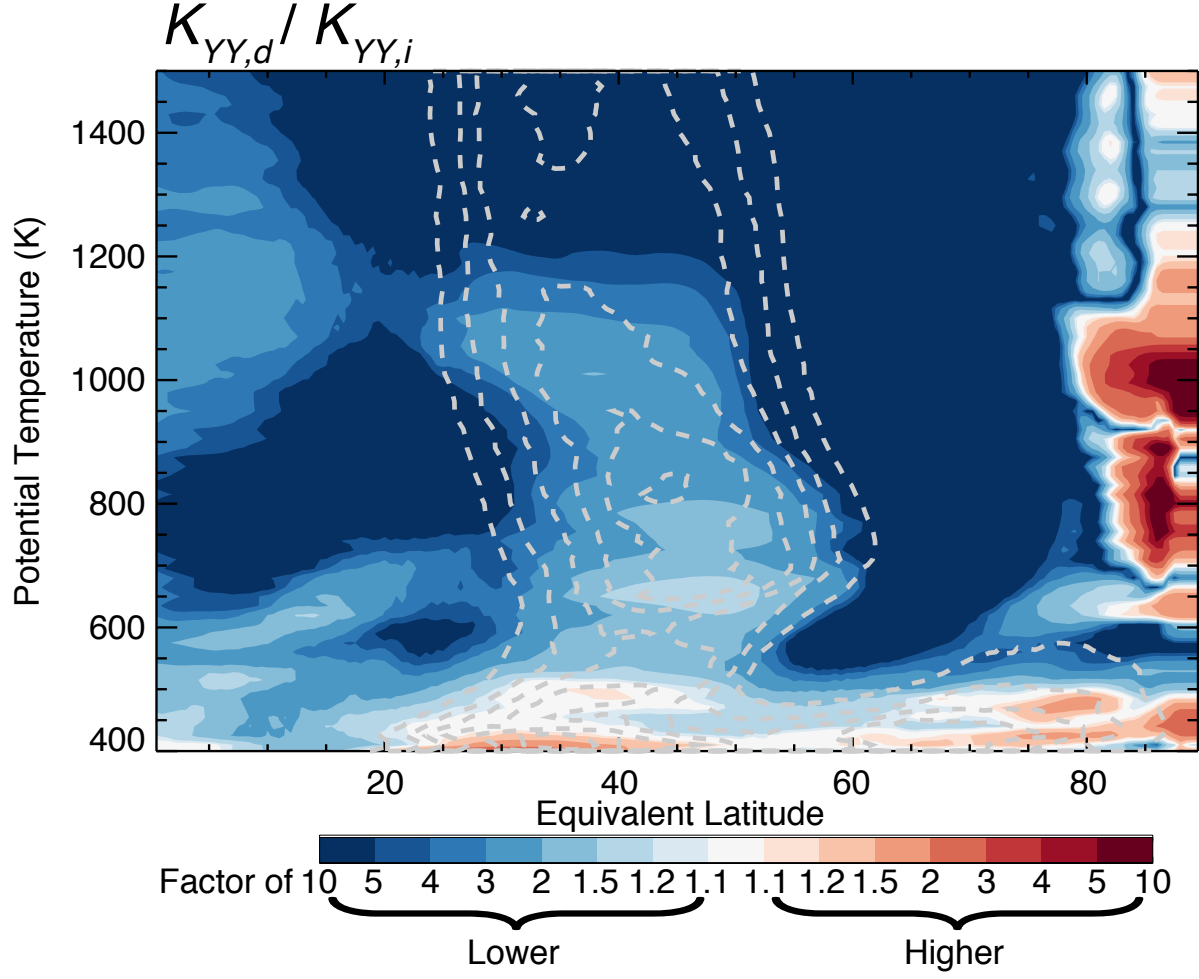


FIG. 4. Ratio of  $K_{YY,d}$  to  $K_{YY,i}$  from the simulation presented in Fig. 3. Blues (reds) indicate that  $K_{YY,d}$  is lower (higher) than  $K_{YY,i}$ .

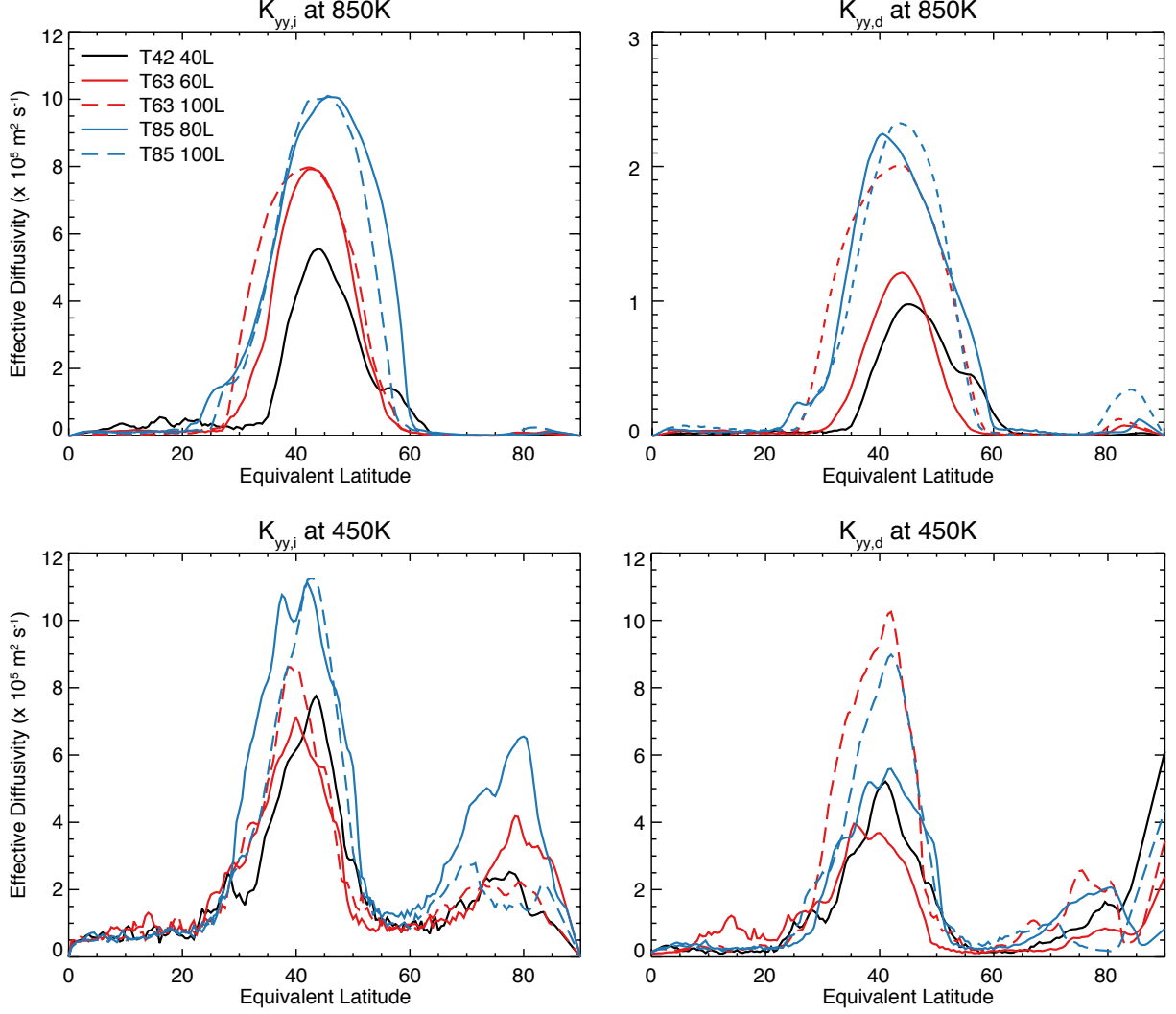


FIG. 5. Effective diffusivity ( $\times 10^5 \text{ m}^2 \text{ s}^{-1}$ )  $K_{YY,i}$  (left) and  $K_{YY,d}$  on the 850K (top) and 450K (bottom) isentropic surface as calculated from simulations with spatial resolutions: T42, 40 levels (black); T63, 60 levels (red line); T63, 100 levels (red dashed line); T85, 80 levels (blue line); T85, 100 levels (blue dashed line). Note the difference in scale between  $K_{YY,i}$  and  $K_{YY,d}$  at 850K.

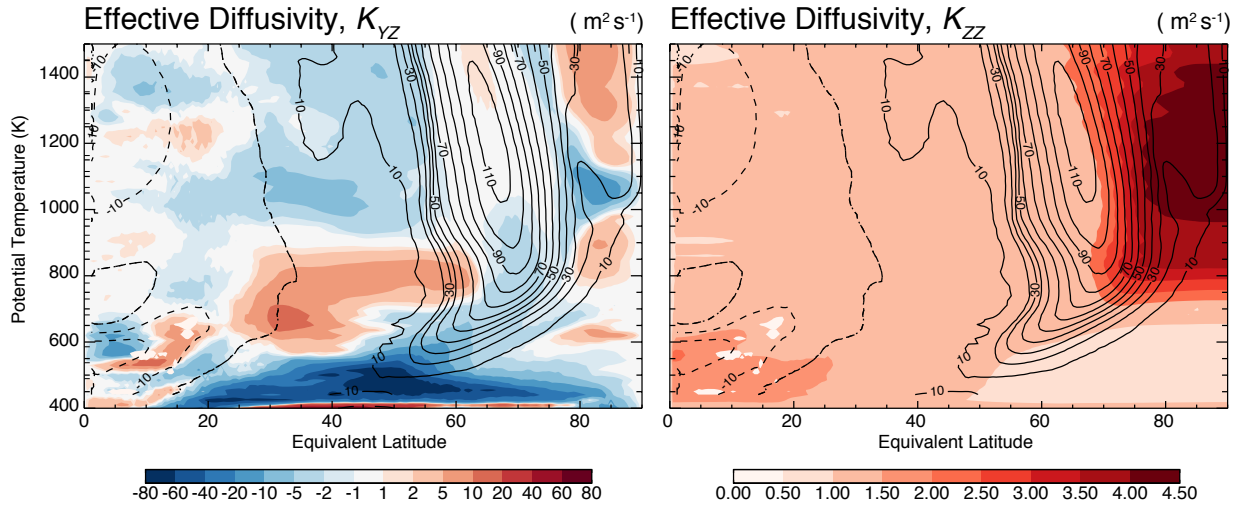


FIG. 6. Effective diffusivity components  $K_{YZ}$  ( $\text{m}^2 \text{s}^{-1}$ ) and  $K_{ZZ}$  ( $\text{m}^2 \text{s}^{-1}$ ) calculated from a simulations dissipating tracer variance with explicit diabatic diffusion  $\kappa$ . Black contours represent the MLM of the zonal wind ( $\text{m s}^{-1}$ ); contour levels are spaced 10  $\text{m s}^{-1}$  apart and negative values are dashed. Note the nonlinear colorscale of  $K_{YZ}$ .

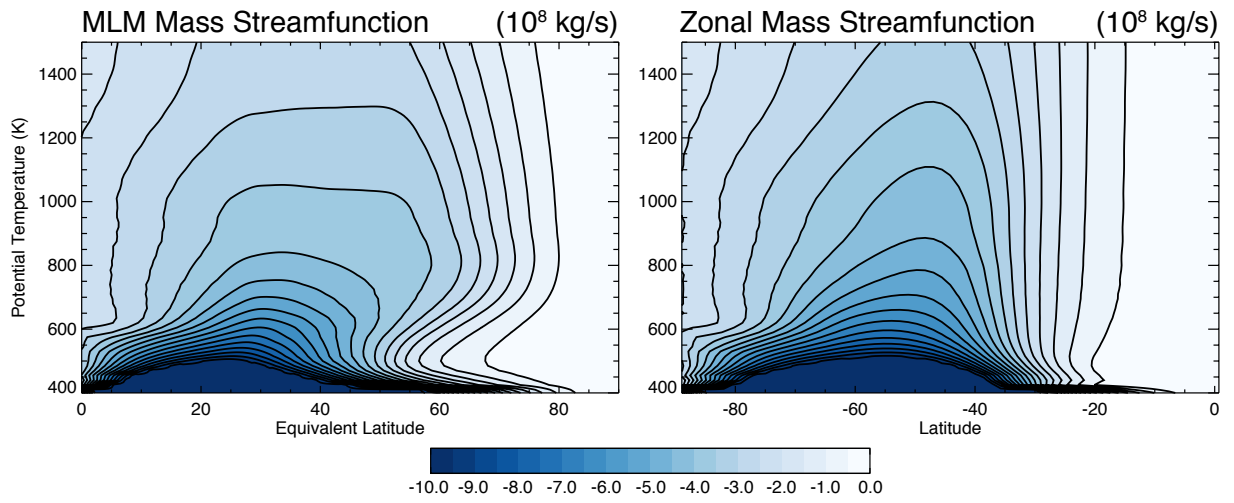


FIG. 7. Mass streamfunctions calculated relative to tracer contours (*i.e.*, equivalent latitude; left) and latitude circles (right).